Sensitivity Enhancement of Surface Plasmon Resonance Biosensor with 2-D Franckeite Nanosheets

Bhishma Karki[1] · Sandeep Sharma[2,3,4] · Yadvendra Singh[5] · Amrindra Pal[6]

Abstract

The sensitivity of a standard surface plasmon resonance (SPR) biosensor in angular interrogation is low. A unique 2-dimensional substantial heterostructure, franckeite/graphene layer, has been deposited over the metal surface to improve the sensitivity; moreover, the sensitivity is limited to a certain extent. A SPR biosensor based on modified Kretschmann configuration has been investigated, contain bimetallic layers of silver (Ag) and nickel (Ni). A layer of franckeite is sandwich in the metal layer. The proposed configuration has a maximum sensitivity of 352°/RIU, which is 80.80% higher than the conventional sensor. The franckeite is an air-stable 2-D material and has application in the chemical, biological, and medical fields.

Keywords Surface plasmon resonance · Chemical sensor · Finite element method (FEM) · Sensitivity enhancement

Introduction

Biosensing applications are becoming popular as the sensing capabilities of the biosensors are enhanced due to the rapid advancements in related technology. Among many available biosensors, surface plasmon resonance (SPR)-based sensing stood out to be an outstanding contender offering high sensitivity, label-free detection along with reliable outcomes for biosensing applications (chemical and biological parameters). An SPR biosensor is suitable for the study of the biological macromolecules, and it also has a wide range of applications in biochemical analysis and detection, food safety [1–3], environmental detection, a biological investigation [4, 5], and gas detection [6, 7].

SPR is an optical excitation of surface plasmon wave (SPW), also referred to as surface plasmon polaritons (SPP) or surface plasmons (SP), at the metal–dielectric interface. The underlying principle of SPR is based on an evanescent wave (EW) and SPs. SP can be seen as an electron cloud wave (or an electromagnetic wave) that moves along the surface of the metal by the contact of the freely oscillating photons and electrons on the surface of metal [8, 9], with an exponentially decaying electric field in both the metal and dielectric mediums. This movement heavily relies on the dielectric refractive index, thus providing high sensitivity to record changes in the analyte refractive index (RI) of the binding events.

The SPW is the transverse magnetic (TM) polarized wave propagating along the interfacing plane that may be induced by p-polarized light. When a p-polarized electromagnetic (EM) wave enters a dielectric media through a prism and, in turn, a metallic layer, an EW is observed at the interface of the two media, ensuring the absorption of energy from the incident light to excite the SPs at this interface. Essential conditions for SPR to be observed are firstly the exact matching of the surface plasmon wave vector (SPWV) and the evanescent wave vector (EWV) [10]. Secondly, the wave is incident at SPR angle or resonance angle. This specific angle of incidence/wavelength is the angle where minima of the reflected light intensity (prism base) are observed due to attenuated total internal reflection (ATR), inciting SPs to couple with incident p-polarized EM Wave at the metal surface [11].

There are two types of SPR sensors, namely, prism based [12] and optical fiber based [12]. In SPR sensors, the

✉ Amrindra Pal
amrindra.ieee@gmail.com

1 Department of Physics, Tri-Chandra Multiple Campus, Tribhuvan University, Kathmandu 44600, Nepal

2 OMKARR Tech, New Delhi, India

3 iNurture Education Solutions, Karnataka, Bengaluru, India

4 Department of IT, Ajeenkya DY Patil University, Pune, Maharashtra, India

5 Applied Plasmonics & Photonics Lab, Indian Institute of Technology Roorkee, Roorkee, Uttarakhand, India

6 Department of EECE Deptt, DIT University, Dehradun, Uttarakhand, India

prism-based technique is commonly deployed. Based on the attenuated total reflection (ATR) [13], two geometric configurations, namely, Kretschmann's–Raether [13] and Otto [14], are employed for prism coupling.

Because of the ease of practical implementation, Kretschmann's geometry/configuration is preferred for SPR applications [15–17]. This configuration conventionally has a single metal film-coated at one end of the glass prism or coated with an air gap between a prism and this metal film, leading to low sensitivity. The objective of the biosensor designer is to increase the momentum of the incoming photon and excite the coupling of the SP to analyte. The analyte attachment to the sensor's surface holds the key for accurate and enhanced performance for the sensors. The SPR is generally controlled by either wavelength [18, 19], or angular interrogation [12, 20] of the incidence light.

The reflectance curve provides sensing performance of the SPR sensor, and it displays reflectivity versus angle of incidence. Generally, Au or Ag is the preferred choice of metal [21]. Au has a low oxidation coefficient but offers a lower absorption rate for biological molecules [22], renders reduced biosensor sensitivity. In contrast, Ag provides higher sensitivity, but it is highly susceptible to oxidation [14], leading to poor sensitivity in the end. One way to prevent Ag oxidation is to substitute a single layer Ag film with a bimetallic film [23–26], and this indeed improves sensors performance by rendering the Ag surface chemically inert [27]. Au produces a larger SPR resonant angle shift on a reflection curve, while Ag has a narrower peak, attributed to a higher value of Ag's dielectric constant (real part).

Sensitivity is a key performance indicator for any sensor. Different biosensors have been proposed in recent decades [28, 29]. With the recent advancement in the technology of 2-D materials, transition metal dichalcogenides (TMDCs) (MoS_2, WS_2, $MoSe_2$, WSe_2) and graphene are used as biorecognition element (BRE), and they have shown to enhance the performances of SPR sensors. Lin et al. [30] reported a biosensor using a few layers of gold, molybdenum disulfide (MoS_2), and graphene with a sensitivity maximum of 182°/RIU. Here gold is used as a metal layer, and it has a lower absorption ability with the biological molecules. Srivastava and Prajapati [21] designed a biosensor based on blue phosphorene/MoS_2 and achieved the highest sensitivity of 230.66°/RIU. Wu et al. [31] proposed a biosensor structure along with a few-layer of black phosphorus and graphene/TMDCs with enhanced sensitivity of 279°/RIU.

In particular, graphene has attractive properties such as tunable electrical and optical characteristics [32], ring-type carbon structure, and high surface-to-volume ratio. Thus, the adsorbates can easily interact with this structure, increasing the adsorption suitable for biosensors [33, 34]. Graphene can be made to be a monolayer or multiple layers via Van der Waal (VDW) force between the layers. VDW heterostructure

[35]-based sensors exist in both natural and artificial forms. The synthetic materials are made using different 2-D materials selectively stacked [31–36], and the natural materials are layered minerals from the sulfosalt family [37–39].

While the sensitivity of the biosensor based on these artificially designed heterostructure(s) can be high, as in those mentioned above, it is not easy to control the lattice orientations. Consequently, undesired atmospheric adsorbates between the layers occur [40]. On the other hand, naturally occurring layered minerals such as Franckeite (member of the sulfosalt family), which is alternating stacks of PbS-like pseudotetragonal (Q) layer and SnSe-like pseudohexagonal (H) layer, are found to possess naturally VDW superlattices [37–39], and it is free from surface contaminations in contrast to the artificially designed heterostructure(s).

Franckeite is a 2-dimensional p-type material, and it can be exfoliated into layers mechanically [41]. It has a crystalline structure and is reported to be stable in the air. Franckeite has a narrow energy band gap of less than 0.7 eV; it can be an alternate material for graphene and black phosphorus, which also have a narrow bandgap. The franckeite nanosheet has been found to have great potential in optoelectronic devices [41, 42]. Gan et al. [43] have designed a franckeite-based SPR sensor using a layer of Ag and a few layers of graphene. The sensitivity for this is obtained as high as 188°/RIU.

In this work, a bi-metallic structure having a sandwiched franckeite layer between the Ag/Ni layers with a graphene-coated adsorbate interface based on Kretschmann's configuration is proposed. It has been shown to enhance the sensitivity of the biosensor. The work also demonstrates the sensitivity of the sensing layers RI depending upon the number of layers of 2-D materials (franckeite and graphene).

The rest of the article is structured as follows. Biosensor theoretical modeling and its design are demonstrated in "Theoretical Modeling and Design Analysis." "Results and Discussions" presents our modeling results and discussion. "Conclusion" provides the conclusion of this work.

Theoretical Modeling and Design Analysis

Figure 1 depicts our design of the SPR biosensor in a typical Kretschmann configuration. The TM polarized optical signal of 633 nm is incident at one surface of the BK7 prism, and the refracted optical signal is received at the other end.

The prism is coated with a thin layer of Ag (a single layer of thickness $w_1 = 50$ nm), which in turn is covered by a 2-D franckeite nanosheet (thickness $w_2 = M * 1.8$ nm where M is an integer with values 0, 1, 2, etc. M represents the number of franckeite layers), followed by a Ni thin film (single layer of thickness $w_3 = 10$ nm). Ni layer is coated with layer(s) of graphene (thickness $w_4 = N * 0.34$ nm, where N is an integer
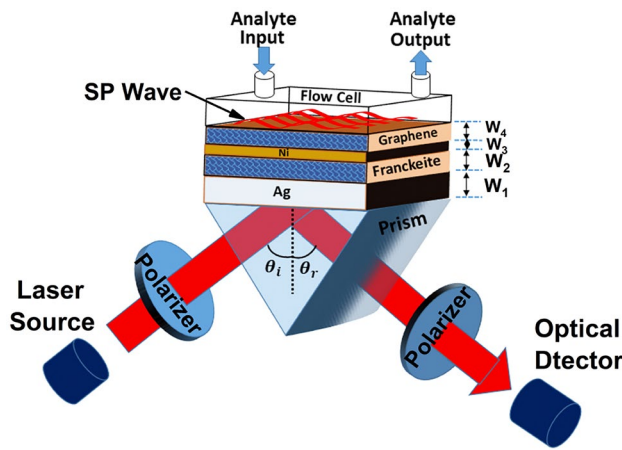
Fig. 1 Layered structure of biosensor based on franckeite

with values 0, 1, 2, etc. N represents the number of graphene layers). The graphene layer is sandwiched between Ni film and the sensing layer. The graphene layer improves the macromolecular captivation of the sensor. The BK7 prism is used as a coupling prism; the RI of the prism is given as

$$n_{pBK7} = \sqrt{1 + \frac{\alpha_1 \lambda^2}{\lambda^2 - \beta_1} + \frac{\alpha_2 \lambda^2}{\lambda^2 - \beta_2} + \frac{\alpha_3 \lambda^2}{\lambda^2 - \beta_3}} \quad (1)$$

where λ is the wavelength of the applied optical signal. The values of the constants $\alpha_1, \alpha_2, \alpha_3, \beta_1, \beta_2$ and β_3 are 1.03961212, 0.231792344, 1.01046945, 0.00600069867, 0.0200179144, and 103.560653, respectively [44]. The RI of the metal layer (Ag) is expressed using the Drude model, $n_{Ag, Ni} = \sqrt{1 - (\lambda^2 \lambda_c)/[\lambda_p^2(\lambda_c + i\lambda)]}$, where $\lambda_c = 17.614 \mu m$ and $\lambda_p = 0.14541 \mu m$ [11, 12, 19, 23]. Similarly, the RI for Ni is obtained using the above formula with $\lambda_c = 0.28409 \mu m$ and $\lambda_p = 0.25381 \mu m$. λ_c and λ_p are the plasma and the collision wavelength for silver and nickel, respectively. The RI (n_f) of franckeite at 1.8-nm thickness is $3.53 + i * 0.39$ in the visible range [12, 13, 20, 26]. The RI of graphene is given as $n_G = 3.0 + iC_1 * \lambda/3$ with $C_1 \approx 5.446 \mu m^{-1}$; λ is the wavelength of the applied optical signal [20, 26]. The RI of the sensing layer is taken $n_s = 1.33$ [12, 13].

Detailed numerical analysis by varying thickness of metal layers was carried out and simulated to get minimum

reflectance for the geometry so that optimal thicknesses (for maximum sensitivity) of metals including silver and nickel, layers can be found. The sensing performance of the systems is estimated using the Fresnel equations [7, 20]. The reflectance is estimated with the formula: [12, 13, 20, 26].

$$r_{pm_1 d_1 m_2 d_2} = \frac{r_{pm_1} + r_{m_1 d_1 m_2 d_2} e^{2iK_{m_{1x}} d_{m_1}}}{1 + r_{pm_1 d_1 m_2 d_2} e^{2iK_{m_{1x}} d_{m_1}}} \quad (2)$$

where

$$K_{ix} = \left(\left(\frac{2\pi}{\lambda} \right)^2 \varepsilon_i - K_z^2 \right)^{1/2}; i = p, m_1 d_1 m_2 d_2$$

$$r_{pm} = \frac{(\varepsilon_m K_{px} - \varepsilon_p K_{mx})}{(\varepsilon_m K_{px} - \varepsilon_p K_{mx})}; r_{md} = \frac{(\varepsilon_d K_{mx} - \varepsilon_d K_{dx})}{(\varepsilon_d K_{mx} - \varepsilon_m K_{dx})}$$

In the subscribes, prism is denoted by p, metal by m, and dielectric by d, respectively.

The dip in the resonance curve can be written as [7, 20]

$$K_{sp} = \frac{2\pi}{\lambda} n_0 \text{Sin} \theta_{SPR} = \text{real} \left(\frac{2\pi}{\lambda} \sqrt{\frac{\varepsilon_m \varepsilon_s}{\varepsilon_m + \varepsilon_s}} \right) \quad (3)$$

n_0 is the RI of the coupling prism; ε_s and ε_m are dielectric constants of the sample and metal, respectively; angle of resonance is θ_{SPR}; and K_{sp} is the propagation constant. The reflectance is defined as $R_P = \left| r_{pm_1 d_1 m_2 d_2} \right|^2$, where $r_{pm_1 d_1 m_2 d_2}$ denotes the reflection coefficient of the incident optical signal. Sensitivity is represented as $S_n = \delta\theta_{SPR}/\delta n_s$, where $\delta\theta_{SPR}$ and δn_s represent the change in the resonance angle and the change in RI of the sensing layer respectively. The consolidated design parameters for the implemented biosensors are listed in Table 1.

Results and Discussions

To achieve high sensitivity, the coupling prism should offer a low refractive index [44]. The prism made of BK7 material suits this description [45]. The prism made from higher refractive index materials provides very sharp

Table 1 Designing parameters for the implemented biosensor

Film of the materials	Used material	RI of the material at 633 nm		Thickness (nm)
		Real part (n)	Imaginary part (k)	
Layer I	Prism BK7	1.5151	-	-
Layer II	Ag (Metal)	0.056253	4.2760	$w_1 = 50$
Layer III	Franckeite	3.53	0.39	$w_2 = M * 1.8$
Layer IV	Ni (Metal)	1.9900	4.1103	$w_3 = 10$
Layer V	Graphene	2.4105	-	$w_4 = 0.34 * N$

resonance curves compared to those with lower refractive indices. However, the prism made from lower refractive index materials provides values of full width half maximum (FWHM), SPR angle, angular shift, and sensitivity that are larger than higher ones [44]. For higher figure of merit and a deep SPR curve, the flat end of the prism was coated with 50-nm-thick silver film. The different number of franckeite layers on top of the Ag film was studied to examine its effect on the structure's sensitivity. The franckeite layer(s) were coated with a 10-nm nickel film. Ni was chosen for several reasons. It acts as a protective layer to prevent Ag from oxidizing rapidly at room temperature. It also acts as a high RI layer, and it can facilitate enlargement of multi-layer graphene grains by suppressing the nucleation of these multi layers as reported by Murata et al. [46]. Finally, the structure was coated with graphene layer(s) to improve the adsorption rates of the analyte with the biosensor.

Figure 2 shows the enhanced performance of sensitivity where reflectance is plotted against the incident angle for various refractive indices of the sensing layers. Figure 2a shows a conventional sensor with no layers of franckeite or graphene in the biosensor, i.e., corresponding to $M = N = 0$. The sharp downfall in the reflectance curve found in the range of specific angles is attributed to the SPR excitation, describing the absorption of incident light by the sensor due to the generated SPs. The resonance dip has small excursion $\delta\theta_{SPR} = 0.99°$, showing that the change in the RI of the sensing layer (contact layer) due to molecular interaction is very low. The sensitivity obtained was 198°/RIU for this conventional sensor. The traditional sensor in Fig. 2a is modified by adding a single graphene layer (no franckeite layer added that is for $M = 0$ and $N = 1$), retaining all other parameters. An increase in both the resonance offset dip as well as sensitivity was observed with values $\delta\theta_{SPR} = 1.03°$ and 206°/RIU, respectively. These values are higher when compared with the values of the conventional biosensor ($M = N = 0$). The enhanced sensitivity and the increase in resonance curve offset dip in this structure are attributed to the higher adsorption rates due to the large surface area and rich π conjugation structure offered by graphene, making it the appropriate choice for dielectric top layer SPR sensing applications [32, 46].

Further investigating the impact of single-layer franckeite with no graphene layers added ($M = 1$ and $N = 0$), again an increase in both the resonance offset dip as well as sensitivity was observed with values $\delta\theta_{SPR} = 1.17°$ and 234°/RIU (Fig. 2c), respectively. These values are better than both the cases that are the conventional biosensor as well as the modified conventional biosensor with single-layer graphene (no layer of franckeite); this enhanced performance is attributed to the narrow bandgap of the franckeite material and better absorption efficiency as compared to graphene (single layer) [37–42].

Another scenario was evaluated for the impact by introducing a single layer of franckeite and a monolayer of graphene in the biosensor ($M = N = 1$). This resulted in significant shifts and a dip in the resonance curve. The resonance

Fig. 2 Plot of reflectance vs. incident angle at same RI with $M = 0$ and $N = 0$ (**a**), $M = 0$ and $N = 1$ (**b**), $M = 1$ and $N = 0$ (**c**), and $M = 1$ and $N = 1$ (**d**)
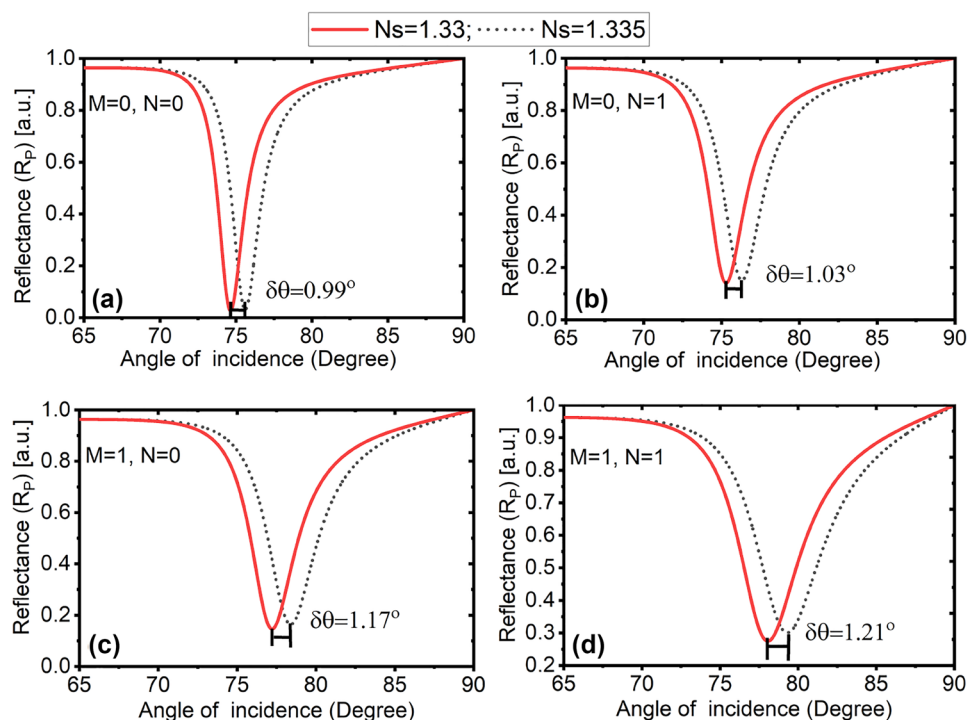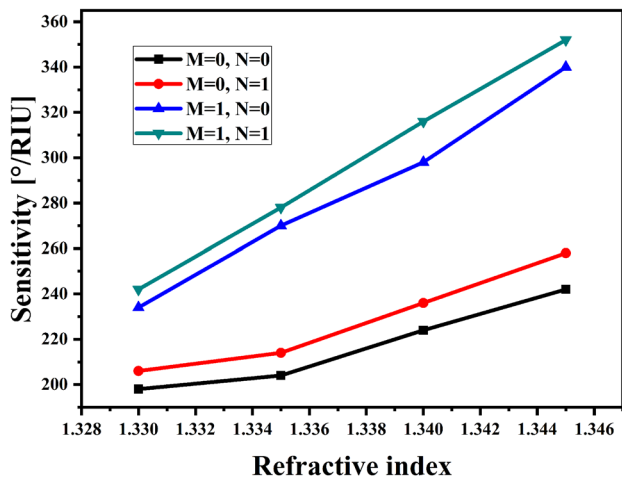
Fig. 3 Variation in sensitivity of sensor w.r.t. RI

angle was obtained as $\delta\theta_{SPR} = 1.21°$, whereas the sensitivity was 242°/RIU as depicted in Fig. 2d. This comparative study reveals that the resonance angle offset increases with the addition of a single layer of graphene, a single layer of franckeite, compared to the conventional sensor. The best results were obtained by adding a single layer of graphene and a single layer of franckeite.

Upon further addition of layers of frankiete and/or graphene (for values of $M \geq 2$ and or $N \geq 2$), increase in the reflectance was observed as depicted in Fig. 4. Thereby makes it difficult to measure accurate resonance angle in the dip; this lowers the sensitivity. The above discussions indicate that the sensitivity of the sensor depends on the RI of the sensing layer. A plot of sensitivity versus RI of the sensing layer (as depicted in Fig. 3) helps understand the impact of various combinations of addition of franckeite and graphene layers. The range of the RI was taken from 1.33 to 1.345. From Fig. 3, it is also evident that there is a significant variation in sensitivity due to the corresponding variation in the RI. The sensitivity varies from 198 to 242°/RIU for $M = N = 0$ to 1, whereas for the case $M = 0$ and $N = 1$,

the sensitivity varies from 206 to 258°/RIU; likewise for $M = 1$ and $N = 0$, the variation from 234 to 335°/RIU was observed. Hence, it can be concluded that the sensitivity increase in the case of the addition of the franckeite sheet is better than that due to the graphene sheet, attributed to the higher optical absorption efficiency of franckeite with respect to graphene. The sensitivity of the biosensor ranges from 242 to 352°/RIU due to the addition of both the single layer of franckeite and single layer of graphene ($M = N = 1$). This justifies the addition of both franckeite and graphene layers to further enhance sensitivity compared with the conventional biosensor.

The analysis provided above shows that the use of franckeite and graphene sheets supports enhancement in the sensor's sensitivity. The number of layer(s) in the structure of the biosensor 2-D materials is varied to analyze the effect of this change in the sensitivity. Figure 4a shows the impact of franckeite nanosheets on the sensitivity of the biosensor. As is evident that with the introduction of several franckeite sheets, reflectance increases. Thus, the reflectance dip transfers to a larger incident angle and broadening of the SPR curve.

Similarly, the effect of the change of the graphene layer on the sensitivity is given in Fig. 4b. A similarity in results with franckeite is observed. The reflectance dip transfers to a larger incident angle, and the broadening of the SPR curve takes place as the number of graphene layers is increased from 1 through 4. Thus, for analysis purposes, the values of M and N are confined to 0 and 1. For the value M and $N = 2$ (and higher), it was observed that the shift in reflectance curve for various values of refractive indices of sensing layer was either overlapping or one of the reflectances was over 0.5 makes. It is challenging to measure accurate resonance angle in the dip for these values and lower sensitivity. Upon further analysis of the results as reported in Fig. 4a, b, it can be observed that the resonant angle offset is more affected by the increase in the number of franckeite nanosheets than the corresponding increase in the number of graphene layers. Also, it can be further inferred that the collective addition

Fig. 4 a, **b** Change in the reflectance w.r.t incident angle: **a** variation in the number of franckeite layers at one graphene layer and **b** variation in the number of graphene layers at one franckeite
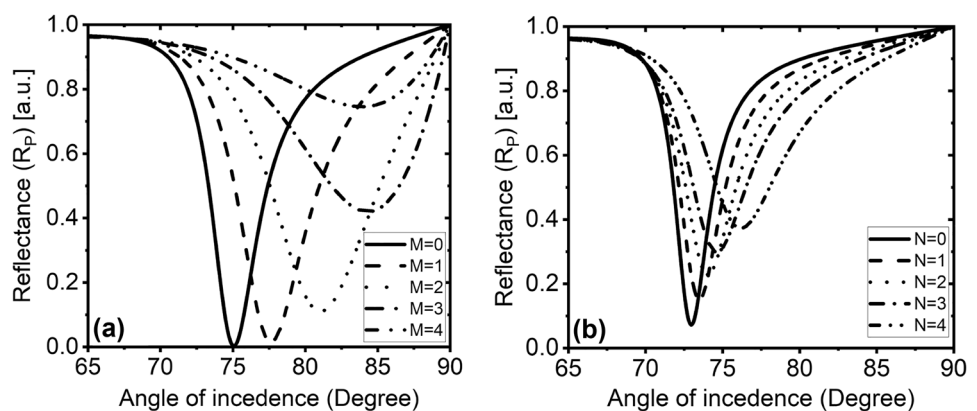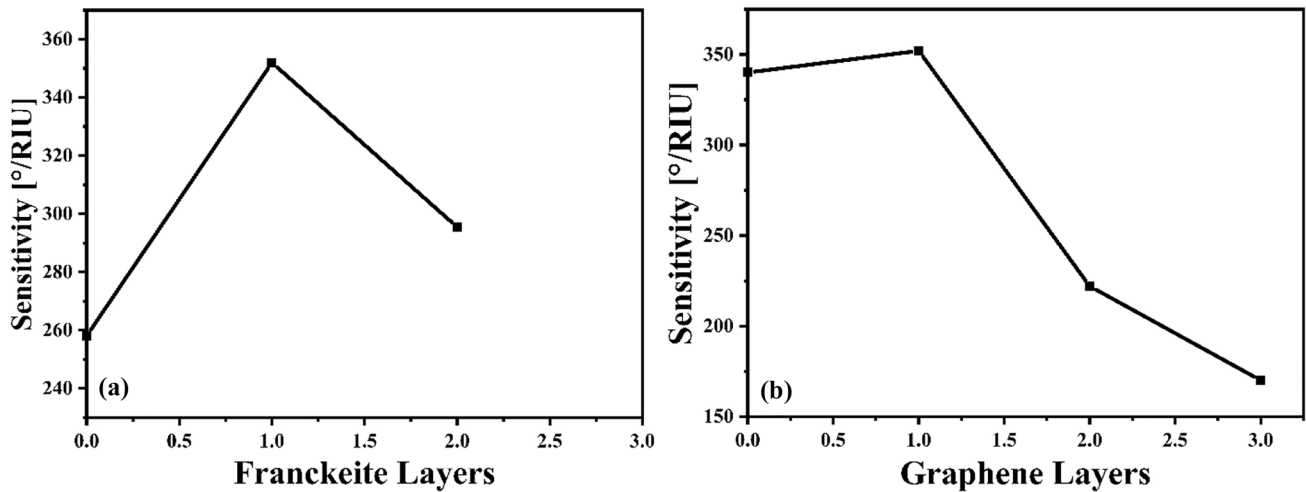
Fig. 5 Change in sensitivity w.r.t. to **a** variation in the number of franckeite layers at one graphene layer and **b** variation in the number of graphene layers at one franckeite

from single franckeite nanosheet and single graphene layer to multiple franckeite nanosheets and multiple graphene layers leads to worsening of the outcome as explained earlier.

Optical energy loss is more due to the increase in the number of franckeite layers than due to the corresponding increase in the graphene layer. From Fig. 5a, b, it can be clearly seen that the sensitivity of the biosensor first improves (the case of adding a single layer of graphene and single layer of franckeite nanosheet) and then significantly decreases with an increase in the number of layers of graphene and franckeite layers increased either individually or collectively. The imaginary RI part for graphene (non-zero) and amortization in the absorption of SP at the Ni/graphene interface [22, 47, 48] causes damped extension of SP field inside the graphene layer resulting in more insufficient sensitivity or detection accuracy or increase in reflectance. This can be visibly seen in the breadth of the SPR curve.

The analysis was carried out for 633-nm wavelength light source. The analysis aptly supports for optical signals at other wavelengths. Table 2 depicts the comparative analysis with the existing work reported in the literature, clearly indicating that the proposed structure offers by far the best sensitivity to the compared structures. The proposed biosensor is highly sensitive for chemical, medical diagnosis, and biological mass detection.

The entire analysis was carried out with the help of the finite element method (FEM) using COMSOL Multiphysics and MATLAB software. In this paper, the electric field enhancement between different layers has been analyzed, and the thickness of the bimetallic (Ag/Ni) layer was also optimized. The electric field analysis provides the confinement of the field at the metal–dielectric interface. It can be noted that the field is well confined at this interface. The coupling of the wave vector at the metal–dielectric interface shows the intensity of the electric field [9]. Figure 6 depicts the density distribution of the electric field X-component with respect to the distance normal to the prism interface for a different number of graphene layers. This electric field distribution verifies the effect of increasing graphene layers on SP field distribution at the graphene-sensing layer interface. As the increasing the number of graphene layers, the sensitivity will decrease. Mathematically, the field intensity enhancement factor (FIEF) is equal to the ratio of the square of the field at graphene–sensing layer interface to the incoming intensity at the prism–metal interface for p-polarized light [7]. Therefore, the FIEF at graphene–sensing layer interface can be obtained by relating the electric field to magnetic field as per Eq. (4) [27].

Table 2 Comparative analysis of the earlier reported work

References	Wavelength (nm)	Used 2-D materials	Minimum sensitivity (°/RIU)	Maximum sensitivity (°/RIU)
[16]	633	Tin selenide	118	178
[43]	633	Franckeite, graphene	116	188
[15]		Graphene, MoS$_2$	183	229
Proposed work	633	Franckeite, graphene	198	352

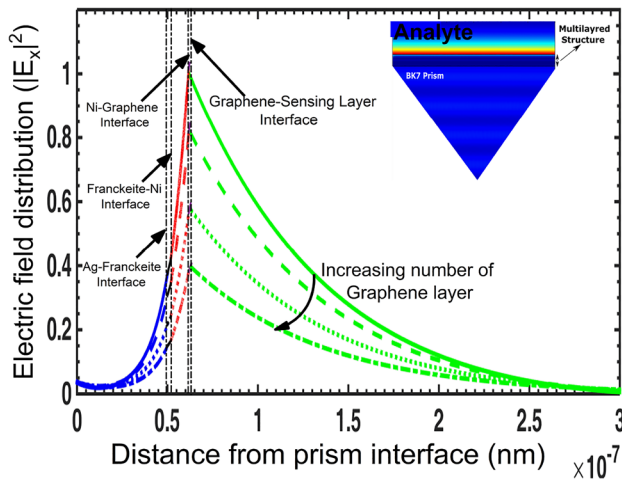**Fig. 6** Electric field distribution inside the biosensor (normalized field)

$$\left| \frac{E_{||}\left(\frac{N}{N-1}\right)}{E_{||}\left(\frac{1}{2}\right)} \right|^2 = \frac{\varepsilon_1}{\varepsilon_N} \left| \frac{H_{y||}\left(\frac{N}{N-1}\right)}{H_{y||}\left(\frac{1}{2}\right)} \right|^2 \qquad (4)$$

Conclusion

An SPR biosensor based on the heterostructure of franckeite nanosheet is proposed for the improvement of sensitivity. In the designed structure, franckeite nanosheet is sandwiched between two metal layers of Ag and Ni with the thickness of 50 and 10 nm, respectively. The investigation carried out in this work reveals that the introduction of franckeite layer(s) and graphene layer(s) in the SPR biosensor in the Kretschmann configuration enhances the sensitivity of the biosensor. Upon further increasing the number of layers from 1 to 2 of graphene and/or franckeite, the 2-D materials tend to exhibit more of metallic nature than semiconducting; this was concluded based upon the enhanced reflection (Fig. 4), thereby broadening the curve and making it difficult to measure accurate resonance angle in the dip for these values. It is also observed that the thickness of the franckeite and graphene layer affects the sensitivity of the biosensor. The sensitivity of the biosensor enhances with the introduction of a single layer of franckeite and a single layer of graphene for individually exclusive as well as collective cases as compared to a conventional sensor. The absorption efficiency of the franckeite nanosheet is more than the graphene layer for separately exclusive single-layer cases. However, using both a single layer of franckeite and graphene layer further improves the sensitivity of the individually exclusive case. The maximum sensitivity of 352°/RIU was observed for the biosensor at a single layer of franckeite and a single graphene layer.

Author Contribution SS formulated the problem statement wherein giving the theoretical background for SPR biosensor. He also helped in drafting the manuscript. YS provided the theoretical background to biosensing and importance of Optical Biosensing. He also helped in reviewing the manuscript. AP provided statistical analysis for the results. He provided the theoretical background to SPR biosensors. He also helped in reviewing and formatting the manuscript. BK worked towards the revision of the complete manuscript, formatting and finalizing the comments of the reviewers.

Declarations

References

1. Neethirajan S, Ragavan V, Weng X, Chand R (2018) Biosensors for sustainable food engineering: challenges and perspectives. Biosensors 8(1):23
2. Ligler FS, Rowe C, Kim LCS, Yura ES, Golden JP (2003) Array biosensor for detection of toxins. Anal Bioanal Chem 377:469–477
3. Mustafa F, Andreescu S (2018) Chemical and biological sensors for food-quality monitoring and smart packaging. Foods 7(10):168
4. Island JO, Steele GA, Van Der Zant HSJ, Castellanos-Gomez A (2015) Environmental instability of few-layer black phosphorus. 2D Mater., 2(1):11002
5. Choi Y, Lee G, Ko H, Wook Y, Kang M, Pyun J (2014) Biosensors and bioelectronics development of SPR biosensor for the detection of human hepatitis B virus using plasma-treated parylene-N film. Biosens Bioelectron 56(15):286–294
6. Xiang Y, Zhu J, Wu L, You Q, Ruan B, Dai X (2018) Highly sensitive terahertz gas sensor based on surface plasmon resonance with graphene. IEEE Photonics J 10(1):1–7
7. Singh Y, Raghuwanshi SK (2019) Electromagnetic wave sensors sensitivity enhancement of the surface plasmon resonance gas sensor with black phosphorus. IEEE Sensors Lett 3(12):1–4
8. Sharma AK (2018) Blue phosphorene/MoS 2 heterostructure based SPR sensor with enhanced sensitivity. IEEE Photonics Technol Lett 30(7):595–598

9. Pal A et al (2020) Prism based surface plasmon resonance biosensor for biomedical applications, in ICOL-2019. Springer Proceedings in Physics 258, Springer Singapore. pp. 1–4

10. Pal A, Jha A (2021) "A theoretical analysis on sensitivity improvement of an SPR refractive index sensor with graphene and barium titanate nanosheets," Optik (Elsevier). 231:166378

11. Homola J (2003) Present and future of surface plasmon resonance biosensors. Anal Bioanal Chem 377(3):528–539

12. Sharma AK, Gupta BD (2006) Theoretical model of a fiber optic remote sensor based on surface plasmon resonance for temperature detection. Opt Fiber Technol 12(1):87–100

13. Kretschmann E, Raether H (1968) Radiative decay of non radiative surface plasmons excited by light, Zeitschrift fur Naturforsch. - Sect. A J Phys Sci. 23(12):2135–2136

14. Otto A (1968) Excitation of nonradiative surface plasma waves in silver by the method of frustrated total reflection. Zeitschrift für Phys 216(4):398–410

15. Nisha A, Maheswari P, Anbarasan PM, Rajesh KB, Jaroszewicz Z (2019) Sensitivity enhancement of surface plasmon resonance sensor with 2D material covered noble and magnetic material (Ni), Opt. Quantum Electron. vol. 51

16. Dai X, Liang Y, Zhao Y, Gan S, Jia Y, Xiang Y (2019) Sensitivity enhancement of a surface plasmon resonance with tin selenide (SnSe) allotropes. Sensors 19(1):173

17. Zhao X et al (2018) Sensitivity enhancement in surface plasmon resonance biochemical sensor based on transition metal dichalcogenides/graphene heterostructure. Sensors 18(7):2056

18. Cappi G, Accastelli E, Cantale V, Rampi MA, Benini L, Guiducci C (2013) Peak shift measurement of localized surface plasmon resonance by a portable electronic system. Sensors Actuators, B Chem 176:225–231

19. Lam WW, Chu LH, Wong CL, Zhang YT (2005) A surface plasmon resonance system for the measurement of glucose in aqueous solution. Sensors Actuators, B Chem 105(2):138–143

20. Lan G, Liu S, Ma Y, Zhang X, Wang Y, Song Y (2015) Sensitivity and figure-of-merit enhancements of liquid-prism SPR sensor in the angular interrogation. Opt Commun 352:49–54

21. Srivastava A, Prajapati YK (2019) Performance analysis of silicon and blue phosphorene/MoS 2 hetero-structure based SPR sensor. PHOTONIC SENSORS 9(3):284–292

22. Wu L, Chu HS, Koh WS, Li EP (2010) Highly sensitive graphene biosensors based on surface plasmon resonance. Opt Express 18(14):14395

23. Pang K, Dong W, Zhang B, Zhan S, Wang X (2016) A performance-enhanced bimetallic chip for the detection of cadmium ions with surface plasmon resonance. Plasmonics 11(4):1119–1128

24. Dyankov G, Zekriti M, Saidi EH, Bousmina M (2012) Long-range surface plasmon supported by asymmetric bimetallic structure. Plasmonics 7(3):479–485

25. Dyankov G, Zekriti M, Bousmina M (2012) Dual-mode surface-plasmon sensor based on bimetallic film. Appl Opt 51(13):2451–2456

26. Jha R, Sharma AK (2009) Chalcogenide glass prism based SPR sensor with Ag-Au bimetallic nanoparticle alloy in infrared wavelength region. J Opt A Pure Appl Opt. 11:045502

27. Ong BH, Yuan X, Tjin SC, Zhang J, Ng HM (2006) Optimised film thickness for maximum evanescent field enhancement of a bimetallic film surface plasmon resonance biosensor. Sensors Actuators, B Chem 114(2):1028–1034

28. Jia Y, Li Z, Wang H, Saeed M (2020) Sensitivity enhancement of a surface plasmon resonance sensor with platinum diselenide. Sensors 20(1):131

29. Ouyang Q, Zeng S, Jiang L, Hong L, Xu G (2016) Sensitivity enhancement of transition metal dichalcogenides / silicon nanostructure-based surface plasmon resonance biosensor. Sci Rep 6:28190

30. Lin Z et al (2016) Tuning and sensitivity enhancement of surface plasmon resonance biosensor with graphene covered Au-MoS 2-Au films tuning and sensitivity enhancement of surface plasmon resonance. IEEE Photonics J 8(6):1–8

31. Wu L et al (2017) Sensitivity enhancement by using few-layer black phosphorus-graphene/TMDCs heterostructure in surface plasmon resonance biochemical sensor. Sensors Actuators, B Chem 249:542–548

32. Rathi S et al (2015) Tunable electrical and optical characteristics in monolayer graphene and few-layer MoS2 heterostructure devices. Nano Lett 15(8):5017–5024

33. Aksimsek S, Jussila H, Sun Z (2018) Graphene – MoS 2 – metal hybrid structures for plasmonic biosensors. Opt Commun 428:233–236

34. Mudgal N et al (2020) BaTiO$_3$-Graphene-Affinity layer–based surface plasmon resonance (SPR) biosensor for Pseudomonas bacterial detection. Plasmonics 15:1221–1229

35. Geim AK, Grigorieva IV (2013) Van der Waals heterostructures. Nature 499(7459):419–425

36. Qin J, Deng L, Xie J, Tang T, Bi L (2015) Highly sensitive sensors based on magneto-optical surface plasmon resonance in Ag/CeYIG heterostructures, AIP Adv. 5(1):1–8

37. Williams TB, Hyde BG (1988) Electron microscopy of cylindrite and franckeite. Phys Chem Miner 15(6):521–544

38. Prando G (2017) Van der Waals heterostructures: the natural way. Nat Nanotechnol 12(3):191

39. Gant P et al (2017) Optical contrast and refractive index of natural van der Waals heterostructure nanosheets of franckeite. Beilstein J Nanotechnol 8(1):2357–2362

40. Molina-Mendoza AJ et al (2017) Franckeite as a naturally occurring van der Waals heterostructure. Nat Commun. vol. 8:14409

41. Velický M et al (2017) Exfoliation of natural van der Waals heterostructures to a single unit cell thickness. Nat Commun 8:1–11

42. Ray K et al (2017) Photoresponse of Natural van der Waals Heterostructures. ACS Nano 11(6):6024–6030

43. Gan S, Zhao Y, Dai X, Xiang Y (2019) "Sensitivity enhancement of surface plasmon resonance sensors with 2D franckeite nanosheets. Results Phys. vol. 13:102320

44. Brahmachari K, Ray M (2013) Effect of prism material on design of surface plasmon resonance sensor by admittance loci method. Front Optoelectron 6(2):185–193

45. Zhan T, Shi X, Dai Y, Liu X, Zi J (2013) Transfer matrix method for optics in graphene layers. J Phys Condens Matter. vol. 25 215301

46. Murata H, Saitoh N, Yoshizawa N, Suemasu T, Toko K (2017) High-quality multilayer graphene on an insulator formed by diffusion controlled Ni-induced layer exchange. Appl Phys Lett 111(24):3–7

47. Maharana PK, Jha R (2012) Chalcogenide prism and graphene multilayer based surface plasmon resonance affinity biosensor for high performance. Sensors Actuators, B Chem 169:161–166

48. Davydov SY, Lebedev AA (2014) Evaluation of the effect of adsorption on the conductivity of single-layer graphene formed on a semiconductor substrate. Phys Solid State 56(12):2580–2583